Simulation of Cellular Changes on Optical Coherence Tomography of Human Retina *

Miriam Santos, Adérito Araújo, Sílvia Barbeiro, Francisco Caramelo, António Correia, Maria Isabel Marques, Luís Pinto, Pedro Serranho, Rui Bernardes, *Member, IEEE*, and Miguel Morgado, *Member, IEEE*

***Abstract*— We present a methodology to assess cell level alterations on the human retina responsible for functional changes observable in the Optical Coherence Tomography data in healthy ageing and in disease conditions, in the absence of structural alterations. The methodology is based in a 3D multilayer Monte Carlo computational model of the human retina. The optical properties of each layer are obtained by solving the Maxwell's equations for 3D domains representative of small regions of those layers, using a Discontinuous Galerkin Finite Element Method (DG-FEM). Here we present the DG-FEM Maxwell 3D model and its validation against Mie's theory for spherical scatterers. We also present an application of our methodology to the assessment of cell level alterations responsible for the OCT data in Diabetic Macular Edema. It was possible to identify which alterations are responsible for the changes observed in the OCT scans of the diseased groups.**

I. Introduction

Optical Coherence Tomography (OCT) has been widely used in ophthalmology for non-invasive structural imaging of the retina. This low coherence interferometry technique [1], also allows to gather functional information from the ocular fundus [2;3] due to its sensitivity to small variations of the refractive index [4]. Our previous studies have established a link between changes in the blood-retina barrier (BRB) and in optical properties of the retina [5], which can be identified by OCT in the absence of structural alterations. Recent work showed that it is possible to discriminate between healthy retinas and retinas of diabetic patients without diabetic retinopathy [5;6], between healthy retinas and retinas of Multiple Sclerosis (MS) patients [6-8] as well as between different age groups of healthy volunteers [9], using classification techniques based just on the statistical information embedded in OCT images, without resorting to any structural information. However, the specific source(s) of those observed differences remain unknown.

For this reason, we decided to develop a computational model of OCT imaging in the retina, capable of simulating the content of OCT data from the human retina. Our long term objective is to understand the changes occurring at the cellular level that lead to differences in OCT data, through the solution of the inverse scattering problem, reconstructing the optical properties of the retinal layers based on their scattering patterns. Reaching this goal requires to assess the direct scattering problem. This comprises two main steps (1) the study of the propagation and scattering of the electromagnetic wave as it travels through the retina and (2) the measurement of scattered light at the detectors. The behavior of light scattering through a scattering tissue can be described by a variety of methods, such as the radiative transfer theory, Lambert's Beer Law, Maxwell's equations and also using statistical approaches like Monte Carlo.

Several approaches have been proposed to describe the interaction of light with retinal tissues. Most are based on single-scattering theory [10], which cannot fully model the complex structure of the retina. This can be achieved by solving Maxwell's equations [11]. The Mie solution to Maxwell's equations is one of the most popular methods to model tissue scattering at the cellular level [12]. However, Mie's solution only describes the scattering patterns for a single homogeneous sphere, therefore limiting its application to scatterers of different shapes and aggregates of scatterers. The Generalized Multiparticle Mie (GMM) introduced by Xu [13] is an extension of Mie's solution to multiple scattering (aggregates of spheres) that models more accurately light scattering from biological tissues. Nevertheless, GMM is also restricted to spherical structures.

More complex models need to be used when considering scatterers of arbitrary shapes. The finite-difference time-domain (FDTD) method is a solution of Maxwell's equations in the time domain that has been applied to a wide range of electromagnetic problems. FDTD has been applied to light scattering from cells [14;15]. This application was further extended to study the influence of different organelles inside the cells. FDTD can model inhomogeneous objects of arbitrary shapes. However, it comprises limitations as well, in particular the computational cost. Due to this, techniques have been developed towards Finite Element Methods (FEM). FEM surpass FDTD methods in terms of geometric flexibility and ability to work with higher orders of accuracy and efficiency in computations.

*This work was supported by the AIBILI - Association for Innovation and Biomedical Research on Light and Image, IBILI - Institute for Biomedical Imaging and Life Sciences and Centro de Matemática da Universidade de Coimbra (CMUC), funded by the European Regional Development Fund through the program COMPETE, and by the Portuguese Government through the FCT - Fundação para a Ciência e a Tecnologia under the projects PEst-C/MAT/UI0324/2013, PEST-C/SAU/UI3282/2013 and PTDC/SAU-ENB/119132/2010.

Miriam Santos and António Correia are with AIBILI-Association for Innovation and Biomedical Research on Light and Image, Coimbra, Portugal

Adérito Araújo, Sílvia Barbeiro and Luís Pinto are with CMUC, Department of Mathematics, University of Coimbra, Portugal,

Francisco Caramelo, Maria Isabel Marques, Pedro Serranho, Rui Bernardes and Miguel Morgado are with IBILI, Faculty of Medicine, University of Coimbra, Portugal.

Pedro Seranho is with Mathematics Section, Department of Science and Technology, Open University, Lisbon, Portugal.

Miguel Morgado is with Department of Physics, University of Coimbra, Portugal (phone: +351 239410639; fax: +351 239829158: e-mail: miguel@fis.uc.pt).

Our approach includes the following steps: (1) build a 3D structural and optical model of small-regions of each retinal layer, (2) solve the Maxwell's equations for each of those 3D domains, using a Discontinuous Galerkin Finite Element Method (DG-FEM) to obtain the scattered field and calculate the scattering cross-section and anisotropy, and (3) use the calculated scattering factors to parameterize a multilayer Monte Carlo model of OCT retinal imaging. To the best of authors' knowledge, this methodology has never been proposed and applied for a complete inverse modeling of OCT data, thus contributing for an important insight on the understanding of retinal changes at a cellular level.

The present manuscript reports on the implementation and analysis of DG-FEM Maxwell 3D model and its validation by comparison with Mie's solution for a single spherical scatterer. We also report on the application of our methodology to model the OCT signal from the Outer Nuclear Layer (ONL) of the retina, for investigating cell level alterations capable of mimicking the OCT signal from the ONL of patients with Diabetic Macular Edema (DME). This layer was chosen as it consistently presents characteristics of DME and also because it may be modeled by approximately spherical scatterers, which helps to simplify the simulation.

DME is a major cause of visual loss in diabetic patients [16]. It is defined as an increased retinal thickness due to fluid accumulation that can be intra- or extra-cellular [17]. In intra-cellular edema, cells have increased fluid intake, becoming enlarged; extra-cellular edema results from fluid accumulation outside the cell, generally as a consequence of the breakdown of the BRB and leakage into the retinal space. In the second type of edema, lipid contents of the leakage can agglomerate into structures called hard exudates.

II. DG-FEM MAXWELL 3D

Here, we present a brief description of DG-FEM Maxwell 3D. This method follows the main ideas presented in [11] for the 2D case.

A. Discontinuous Galerkin method

The DG formulation used in this work follows the nodal formulation described in [18] and its specifications were previously discussed, for the 2D case, in [11]. Now we consider the 3D case and restrict our attention to computational domains (meshes) tessellated by tetrahedrons.

B. Low-storage Runge-Kutta

For time integration, we used the improved fourth-order, 14-stage low-storage Runge-Kutta (LSRK) presented in [19], instead of the fourth-order, five-stage LSRK method used in [18]. This reduces the computational time in 40 %, without further increasing the computational cost, as verified in [11].

C. Domain constraints and specifications

In electromagnetic simulation, and even more for the successful application of the DG method, it is important to account for absorbing boundary conditions. The purpose of specifying such constraints is to avoid undesirable reflections caused by non-absorbing boundary conditions, which invade the simulation domain and interfere with the phenomenon of interest. We consider the perfectly matched layer (PML) formulation in [20].

Furthermore, a variable electric permittivity was introduced to simulate the full complexity of the retina, changing the initial formulations in [18]. Since we are modeling exclusively biological domains, which are magnetically transparent, the magnetic permeability will be considered as a constant ($\mu \approx 1$). To introduce the effect of spatially variable electric permittivity ($\varepsilon \rightarrow \varepsilon(x)$), the numerical fluxes (**E** and **H**) must incorporate the local impedance Z and conductance Y as

$$Z^{\pm}=\frac{1}{Y^{\pm}}=\sqrt{\frac{1}{\varepsilon^{\pm}}}, \quad (1)$$

where the superscript "+" refers to the neighboring element and the superscript "-" refers to the local cell.

D. Near-To-Far-Field Transformation

A well-defined scattered-field region enables the computation of the near-field scattering pattern. However, to simulate the retinal layers, we are interested in the far-field scattering phenomena. Using the near-field data, it is possible to apply a near-field to far-field transformation (NFTFFT) to obtain the far-field scattering pattern [21]. The NFTFFT is an application of the surface equivalence principle: the values of the near-field at a virtual surface surrounding the scatterer are used to compute a magnetic and electric "current" that allows the computation of the scattered field at any point outside the virtual surface.

Knowing the far-field scattering pattern $F_s(\theta,\phi)$, it is possible to determine the macroscopic parameters anisotropy (g) and scattering cross-section (σ_s), defined by:

$$g = \int_0^{\pi} p(\theta)\cos(\theta)\sin(\theta)d\theta, \quad (2)$$

$$\sigma_s = \int_0^{2\pi}\int_0^{\pi} F_s(\theta,\phi)\sin(\theta)d\theta, \quad (3)$$

with $p(\theta)$ the scattering phase function [14].

III. VALIDATION

The validation of DG-FEM Maxwell 3D with Mie's solution, requires a domain composed by spherical cells. In fact, a single spherical cell is considered, simply modeled as a dielectric object. For Mie's solution, we used software based on [22]. For DG-FEM, all mesh generation is done with FreeFem. Before each simulation, the initial mesh is discretized as a cube domain, with two spherical interfaces, which correspond to the scatterer and the surrounding virtual surface where the field's dynamics are collected.

We calculated the differential scattering cross sections $d\sigma/d\theta$, solely depending on the scattering angle (azimuthally averaged), only for unpolarized light. The comparison between Mie's and DG-FEM Maxwell 3D solution was done by calculating the differential cross sections and the relative percentual error between the g and σ_s results. The results are shown in Fig. 1. and 2 and Table I.

The results are within the required precision. However, some aspects need further improvement, mostly regarding the sensibility to the incident wave's frequency, DG-FEM order of interpolation and mesh discretization. Our simulations have shown that an increase in the wave's

frequency requires an increase in the method's order, which is computationally expensive. Furthermore, the quality of the mesh also affects the precision of results and cannot be compensated by increasing the polynomial order. In order to improve the mesh quality and precision while maintaining a reasonable computational time, it could be necessary to further refine the mesh in areas where the electromagnetic fields are expected to be more complex.

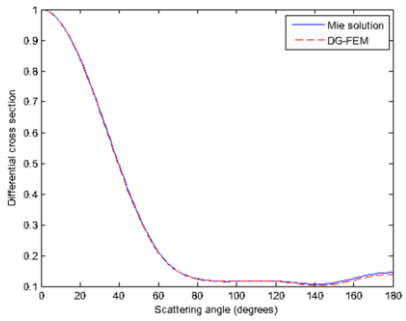

Figure 1. Normalized plot of dσ/dθ for scattering angles up to 180 degrees

TABLE I. COMPARISON OF g AND σ_s FOR BOTH SOLUTIONS

	g	σ_s
Mie's solution	0,72924	2,7367
DG-FEM simulation	0,73193	2,7349
Relative error (%)	0,36794	0,064

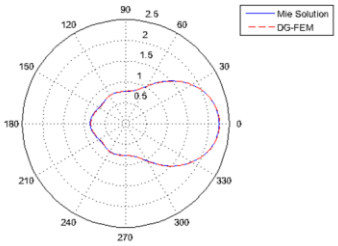

Figure 2. Polar plot of dσ/dθ for all scattering angles

IV. APPLICATION

We applied our simulation tool to the study of DME. OCT scans were acquired from healthy controls and patients with DME. The collected OCT data was divided into three distinct groups: healthy subjects, DME patients with significantly increased ONL thickness (DME I) and DME patients without visible changes in the ONL (DME II). All experimental procedures involving human subjects were approved by the Institutional Review Board of AIBILI.

For each group, the ONL was segmented and processed, yielding a representative OCT A-scan. Using reference values for the physical and optical characteristics of the healthy human retina, we used a Monte Carlo method with a model for the ONL, parameterized with values obtained from DG-FEM Maxwell 3D model, to simulate an A-scan for each group and compare it to the real data.

A. *OCT acquisition and processing*

Optical coherence tomograms (Cirrus HD-OCT, Carl Zeiss Meditec) of eyes diagnosed with DME and eyes of healthy controls were collected from our institutional database to be processed and analyzed. We organized the acquisition information in above groups described.

Several steps are performed from the raw OCT data to the averaged A-scan describing each group. First, the ONL is manually segmented from the original data and all B-scans from a group are aligned to its upper boundary. The segmented data for each group is then averaged into a mean B-scan, which in turn is averaged into a mean A-scan. The resulting scan is normalized by the maximum intensity at the lowest retinal boundary (the retinal pigmented epithelium), thus removing any dependence on above structures/media opacity. The averaged A-scan is then cropped to discard any influence from inaccuracies in segmentation and clipped to the smallest ONL thickness measured.

B. *Model and Monte Carlo simulation*

The ONL is mostly populated by the photoreceptor cell's soma. Thus, we postulate that the main contribution to light scattering in this layer comes from the nucleus, as it presents the highest refractive index difference to the surrounding medium. With this is mind, we modeled the ONL as a population of spherical nuclei in a homogenous medium. This framework allows us to test several optical and physical properties of the cellular medium, namely the nucleus's diameter and refractive index, the medium's refractive index and the nuclei density (number of nuclei per unit volume).

To perform the simulation, we implemented a Monte Carlo method in Matlab, loosely based on the Monte Carlo multilayer method [23] with parameters describing the interaction of light with the medium provided by the DG-FEM Maxwell 3D model. We implemented a photon packet injection following a Gaussian beam shape. The detection scheme is based on the one proposed by Kirilin et al. [24]. Another consideration taken into account was to store the total travel path instead of the photon's deepest length. This allows accounting for multiple scattering and its noise effect, as a multi-scattered photon, if detected, may be mistaken as coming from a depth equal to its total travel path.

The impact of each parameter in the simulated scan was estimated by running multiple simulations of the ONL, modifying one parameter at a time. By matching the various simulated scans with the representative A-scans for each eye group, we could determine which set of parameters can reproduce the collected data

B. *Results*

We were able to simulate adequately both DME groups. In Fig. 3 we compare the simulated and real OCT data for the healthy controls and the two DME groups. There are significant differences between the OCT signals from the two groups. The DME group I has consistently a stronger intensity signal throughout the ONL than the healthy controls. To reproduce this condition, it was mandatory to increase the nuclei's radius by 14% from the healthy status, while keeping all the other parameters unchanged. No other combination of parameters was able to mimic the OCT data.

In the DME group II, the increase in ONL thickness leads to a reduced backscattered signal compared to the healthy status. We were successful in reproducing DME group II's data by decreasing the nuclei density in the simulation. We

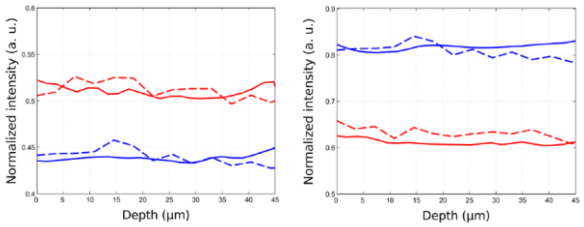

(a) (b)

estimated the nuclei density by assuming that the number of nuclei is unchanged and increasing the simulated ONL's volume according to the ONL's thickness increase from 70.3 μm in the healthy case to 117.2 μm

Figure 3. Comparison between simulated A-scans (dashed lines) and real A-scans (solid lines), both normalized, for healthy controls (blue) and DME groups (red): (a) DME group I; (b) DME group II

V. Conclusions

We proposed a method for solving the time-dependent Maxwell's equations focusing on the simulation of light scattering through the retina's layers, DG-FEM Maxwell 3D. The validation of the proposed methodology was done by comparison with Mie's theory, considering the light scattering for a single sphere. The obtained results are in agreement with those obtained using Mie's theory. The successful validation of our methodology enables the extrapolation of the method to non-spherical structures and opens its application to all retinal layers.

We also presented a first application of our methodology. The results achieved seem to corroborate the existence of two types of edema: cytotoxic (intra-cellular) and vasogenic (extra-cellular). We were able to identify changes at the cellular level that can justify the alterations in the ONL of DME eyes as measured noninvasively by OCT. Although other modifications at cellular level may be responsible for these differences, we discarded variations that were not compatible with the known ocular physiology.

References

[1] P. Serranho, A. M. Morgado, and R. Bernardes, "Optical Coherence Tomography: a concept review," in *Optical Coherence Tomography: A Clinical and Technical Update*. R. Bernardes and J. Cunha-Vaz, Eds. Berlim - Heidelberg: Springer-Verlag, 2012, pp. 139-156.

[2] K. Bizheva, R. Pflug, B. Hermann, B. Povazay, H. Sattmann, P. Qiu, E. Anger, H. Reitsamer, S. Popov, J. R. Taylor, A. Unterhuber, P. Ahnelt, and W. Drexler, "Optophysiology: Depth-resolved probing of retinal physiology with functional ultrahigh-resolution optical coherence tomography," *Proceedings of the National Academy of Sciences of the United States of America*, vol. 103, no. 13, pp. 5066-5071, Mar.2006.

[3] J. A. Izatt, M. D. Kulkami, S. Yazdanfar, J. K. Barton, and A. J. Welch, "In vivo bidirectional color Doppler flow imaging of picoliter blood volumes using optical coherence tomograghy," *Optics Letters*, vol. 22, no. 18, pp. 1439-1441, Sept.1997.

[4] S. S. Abdallah, O. Ramahi, and K. Bizheva, "FDTD Simulation of Electromagnetic Wave Sacttering from Retina Cells," in *Proceedings of the 29th Annual International Conference of the IEEE EMBS* Lyon, France: 2007, pp. 1639-1642.

[5] R. Bernardes, T. Santos, P. Serranho, C. Lobo, and J. Cunha-Vaz, "Noninvasive evaluation of retinal leakage using optical coherence tomography," *Ophthalmologica*, vol. 226, no. 2, pp. 29-36, 2011.

[6] R. Bernardes, "Optical coherence tomography: Health information embedded on OCT signal statistics," *Conf. Proc. IEEE Eng Med. Biol. Soc.*, vol. 2011, pp. 6131-6133, 2011.

[7] T. Santos, L. Ribeiro, C. Lobo, R. Bernardes, and P. Serranho, "Validation of the automatic identification of eyes with diabetic retinopathy by OCT," *Bioengineering. (ENBENG.), 2012. IEEE 2nd. Portuguese Meeting. in*, pp. 1-4, 2012.

[8] R. Bernardes, A. Correia, O. d'Almeida, S. Batista, L. Sousa, and M. Castelo-Branco, "Optical properties of the human retina as a window into systemic and brain diseases," *Invest Ophthalmol. Vis. Sci.*, vol. 55, no. E-Abstract 3367 2014.

[9] R. Bernardes, P. Serranho, T. Santos, V. Gonçalves, and J. Cunha-Vaz, "Optical Coherence Tomography: automatic retina classification throughsupport vector machines," *European Ophthalmic Review*, vol. 6, no. 4, pp. 200-203, 2012.

[10] J. M. Schmitt, A. Knuttel, and R. F. Bonner, "Measurement of Optical-Properties of Biological Tissues by Low-Coherence Reflectometry," *Applied Optics*, vol. 32, no. 30, pp. 6032-6042, Oct.1993.

[11] A. Araujo, S. Barbeiro, L. Pinto, F. Caramelo, A. Correia, M. Morgado, P. Serranho, A. S. C. Silva, and R. Bernardes, "Numerical solution of time-dependent Maxwell's equations for modeling scattered electromagnetic wave's propagation," *Proceedings of the 13th International Conference on Computational and Mathematical Methods in Science and Engineering, CMMSE 2013*, 2013.

[12] S. L. Jacques, "Optical properties of biological tissues: a review," *Phys. Med. Biol.*, vol. 58, no. 11, p. R37-R61, June2013.

[13] Y. L. Xu, "Electromagnetic scattering by an aggregate of spheres," *Appl. Opt.*, vol. 34, no. 21, pp. 4573-4588, July1995.

[14] A. Dunn and R. Richards-Kortum, "Three-dimensional computation of light scattering from cells," *IEEE J. Sel. Top. Quantum Electron*, vol. 2, no. 4, pp. 898-905, 1996.

[15] X. T. Su, K. Singh, W. Rozmus, C. Backhouse, and C. Capjack, "Light scattering characterization of mitochondrial aggregation in single cells," *Opt. Express*, vol. 17, no. 16, pp. 13381-13388, Aug.2009.

[16] T. A. Ciulla, A. G. Amador, and B. Zinman, "Diabetic retinopathy and diabetic macular edema: pathophysiology, screening, and novel therapies," *Diabetes Care*, vol. 26, no. 9, pp. 2653-2664, Sept.2003.

[17] J. Cunha-Vaz and R. Bernardes, "Nonproliferative retinopathy in diabetes type 2. Initial stages and characterization of phenotypes," *Prog. Retin. Eye Res.*, vol. 24, no. 3, pp. 355-377, May2005.

[18] J. S. Hesthaven and T. Warburton, *Nodal discontinuous Galerkin methods: algorithms, analysis, and applications*. New York: Springer-Verlag, 2008.

[19] J. Niegemann, R. Diehl, and K. Bush, "Efficient low-storage Runge-Kutta schemes with optimized stability regions," *J. Comput. Phys.*, vol. 231, pp. 364-372, 2012.

[20] E. Turkel and A. Yefet, "Absorbing PML boundary layers for wave-like equations," *Applied Numerical Mathematics*, vol. 27, pp. 533-557, 1998.

[21] A. Taflove and S. C. Hagness, *Computational Electrodynamics: the finite-difference time-domain method* Artech House, 2005.

[22] J. Schäfer, S. Lee, and A. Kienle, "Calculation of the near fields for the scattering of electromagnetic waves by multiple infinite cylinders at perpendicular incidence," *J. Quant. Spectrosc. Radiat. Transf.*, vol. 113, no. 16, pp. 2113-2123, 2012.

[23] L. H. Wang, S. L. Jacques, and L. Q. Zheng, "Mcml - Monte-Carlo Modeling of Light Transport in Multilayered Tissues," *Computer Methods and Programs in Biomedicine*, vol. 47, no. 2, pp. 131-146, July1995.

[24] M. Kirillin, I. Meglinski, V. Kuzmin, E. Sergeeva, and R. Myllyla, "Simulation of optical coherence tomography images by Monte Carlo modeling based on polarization vector approach," *Opt. Express*, vol. 18, no. 21, pp. 21714-21724, Oct.2010.